

Two-level quantum walkers on directed graphs. I. Universal quantum computingRyo Asaka^{✉,*}, Kazumitsu Sakai^{✉,†} and Ryoko Yahagi^{✉,‡}*Department of Physics, Tokyo University of Science, Kagurazaka 1-3, Shinjuku-ku, Tokyo 162-8601, Japan* (Received 4 May 2022; revised 11 December 2022; accepted 11 January 2023; published 13 February 2023)

In the present paper, the first in a series of two, we propose a model of universal quantum computation using a fermionic or bosonic multiparticle continuous-time quantum walk with two internal states (e.g., the spin-up and -down states of an electron). A dual-rail encoding is adopted to convert information: A single qubit is represented by the presence of a single quantum walker in either of the two parallel paths. We develop a roundabout gate that moves a walker from one path to the next, either clockwise or counterclockwise, depending on its internal state. It can be realized by a single-particle scattering on a directed weighted graph with the edge weights 1 and $\pm i$. The roundabout gate also allows the spatial information of the quantum walker to be temporarily encoded in its internal states. The universal gates are constructed by appropriately combining several roundabout gates, some unitary gates that act on the internal states, and two-particle scatterings on straight paths. No ancilla qubits are required in our model. The computation is done by just passing quantum walkers through properly designed paths. Namely, there is no need for any time-dependent control. A physical implementation of quantum random access memory compatible with the present model will be considered in the second paper [R. Asaka *et al.*, following paper, *Phys. Rev. A* **107**, 022416 (2023)].

DOI: [10.1103/PhysRevA.107.022415](https://doi.org/10.1103/PhysRevA.107.022415)**I. INTRODUCTION**

Quantum walks were introduced as a quantum version of random walks and have since been widely studied in various fields of mathematics, physics, and computer science [1–9]. The time evolution of quantum walks is generated by a reversible unitary process, unlike classical random walks, which evolve according to a stochastic process. Namely, the randomness stems from a quantum superposition state due to a unitary evolution and its collapse into a particular state with a certain probability after an observation or measurement. Due to their remarkable characteristics, most notably fast-spreading properties caused by quantum interference, quantum walks have been employed as quantum algorithms that significantly reduce the computation time for solving practical problems: a search problem [10–12], a hitting time problem [3,12–14], an element distinctness problem [15,16], and a graph isomorphism problem [2,13,17–21].

On the other hand, quantum walks can also be viewed as an architecture of quantum computing. Childs [22] has proposed a novel model of universal quantum computation using a continuous-time quantum walk. A quantum walker evolves continuously in time t but discretely in space, according to a unitary operator $e^{-iA(G)t}$ associated with the adjacency matrix $A(G)$ for an unweighted graph G . An n -qubit state is rep-

resented by a superposition state in 2^n -dimensional Hilbert space, where the basis state is expressed as the presence of a single quantum walker on any of the 2^n semi-infinite paths in G [see Fig. 1(a)]. The universal gates are implemented by single-particle scattering processes on a subgraphs \hat{G} connected to 2^n semi-infinite paths. That is, the outcome of the computation corresponds to the final state of the following process: (i) A quantum walker starts at one of the semi-infinite paths (in superposition) and moves toward \hat{G} , (ii) it scatters on \hat{G} , and (iii) it goes out to some of semi-infinite paths. Shortly after that, Lovett *et al.* extended this idea to a discrete-time version of the quantum walk [24,25].

While universal gates can be constructed via quantum walks, they cannot be straightforwardly utilized as a practical architecture for a quantum computer because of their lack of scalability: 2^n paths are required to express n qubits. [See Fig. 1(a), for example.] To overcome the difficulty, introducing multiparticle continuous-time quantum walks, Childs *et al.* designed a practical model of a quantum computer [23]. They used a so-called dual-rail encoding where a qubit is denoted by the presence of a single quantum walker in either of the two semi-infinite paths [see Fig. 1(b)]. Single-qubit gates are implemented in the same way as the single-particle universal computation. On the other hand, two-qubit gates are realized by a particular combination of single-qubit gates and two-particle scattering of a walker representing the logical qubit from that for the ancilla qubit [see Fig. 6(b) for an implementation of the controlled-phase (CP) gate]. Consequently, the graphs required for the architecture are exponentially smaller than those for single-particle quantum walks. This remarkable progress has been applied to various aspects of quantum computation via quantum walks [26–33].

In another direction of application of quantum walks to quantum computation, the authors of the present paper have

*hello.ryoasaka@gmail.com

†k.sakai@rs.tus.ac.jp

‡yahagi@rs.tus.ac.jp

Published by the American Physical Society under the terms of the Creative Commons Attribution 4.0 International license. Further distribution of this work must maintain attribution to the author(s) and the published article's title, journal citation, and DOI.

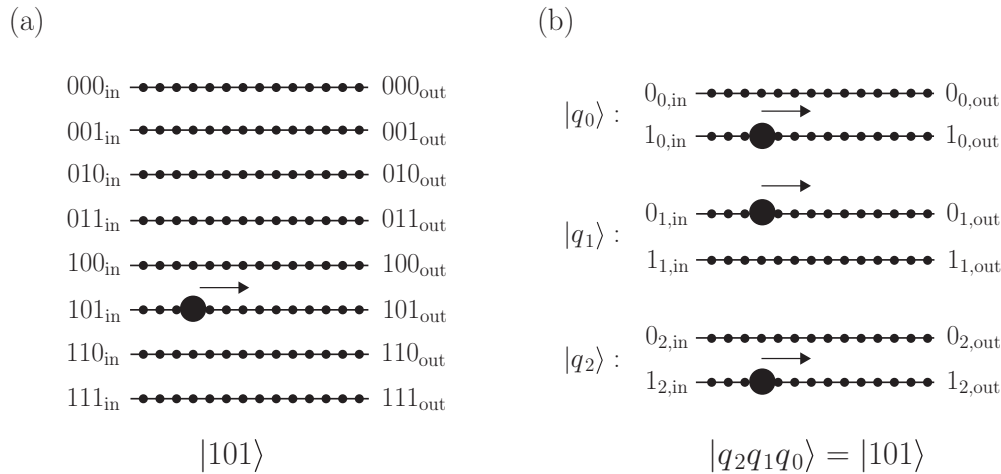


FIG. 1. Information spatially encoded by the presence of a quantum walker. (a) Representation used in a single-particle architecture [22]. 2^n paths are required to express n -qubit information. (b) Dual-rail encoding used in [23] and the present work. In contrast to (a), only $2n$ paths are necessary to represent n -qubit information. Instead, n walkers are required. Both (a) and (b) express the state $|5\rangle = |101\rangle$. See (2.1) and (2.2) for a more precise definition of the dual-rail encoding.

recently proposed a new algorithm for quantum random access memory (QRAM) [34]. A QRAM is a quantum device to access 2^n m -qubit data $|x^{(a)}\rangle_D \in (\mathbb{C}^2)^{\otimes m}$ ($0 \leq a \leq 2^n - 1$) stored in memory cells at addresses $|a\rangle_A \in (\mathbb{C}^2)^{\otimes n}$ and retrieve the data in superposition:

$$\text{QRAM: } \sum_a |a\rangle_A |0\rangle_D \mapsto \sum_a |a\rangle_A |x^{(a)}\rangle_D. \quad (1.1)$$

In our algorithm, QRAM is defined on a perfect binary tree with depth n , where data and addresses are dual-rail encoded by quantum walkers. The walkers moving in QRAM have two internal states, and depending on their states, a device equipped at each node on the tree (hereafter referred to as a roundabout gate) can properly send the walkers to the designated memory cells placed on the leaves of the tree. As a result, our algorithm requires only $O(n)$ steps and $O(n + m)$ -qubit resources to access and retrieve the 2^n m -qubit data. Characteristically, our algorithm promises to require no time-dependent control: QRAM processing is accomplished automatically by simply passing walkers through the binary tree. However, the physical implementation of QRAM, especially how to realize the roundabout gate, has remained a crucial open problem.

The main objectives of the series of two papers are a physical implementation of QRAM using continuous-time multiple quantum walkers with two internal states and a design of a universal quantum computer compatible with this QRAM. The present paper provides a physical implementation of roundabout gates and uses them to provide a universal set of quantum gates. An efficient physical implementation of QRAM will be presented in the following paper [35].

In our scheme, a single qubit is spatially represented by a dual-rail encoding as in the above model [23]. On the other hand, the quantum walker can have two internal states $|0\rangle_c$ and $|1\rangle_c$ (e.g., the spin-up and -down states of an electron), allowing the physical implementation of a roundabout gate and simplifying the architecture. On the graph G , the quantum walkers evolve according to $e^{-i\mathcal{H}_G t}$, where \mathcal{H}_G is the

Hamiltonian associated with the adjacency matrix $\mathcal{A}(G)$ and its complex conjugate $\mathcal{A}(G)^*$. In contrast to the model in [23], single-particle scattering on a subgraph \hat{G} is used only to implement the roundabout gate that moves a walker clockwise or counterclockwise from one path to the next, depending on the internal state of the walker. A feature of this model is that the roundabout gate also allows the spatial information of the quantum walker to be temporarily encoded in its internal states. Some single-qubit gates are implemented by devices equipped along linear paths, acting on the internal states of walkers. The internal states $|0\rangle_c$ and $|1\rangle_c$ of a walker may coexist only at the moment when the walker passes through a single-qubit gate, and its coherence is completely independent of the other gates.

To implement the roundabout gate, we must consider a scattering on a directed weighted graph \hat{G} , which is equivalent to imposing an internal-state-dependent phase factor on the Hamiltonian \mathcal{H}_G . That is, in the subgraph \hat{G} , a walker with $|0\rangle_c$ is evolved by $e^{-i\mathcal{A}(\hat{G})t}$, while a walker with $|1\rangle_c$ is evolved by $e^{-i\mathcal{A}(\hat{G})^*t}$. This difference allows for the implementation of the roundabout gate. A two-qubit gate is simply realized by an appropriate combination of roundabout gates, single-qubit gates, and two-particle scatterings of fermionic or bosonic walkers with the same internal state. [For instance, see Fig. 6(a) for the CP gate.] Notably, the calculation is achieved by simply passing quantum walkers through adequately designed paths; there is no need for any time-dependent control. Furthermore, any ancilla qubit required in the model of [23] to implement the two-qubit gates is unnecessary for our architecture. Consequently, we can simplify the architecture compared to the model in [23].

The remainder of the paper is organized as follows. In the subsequent section, we define continuous-time multiple quantum walkers with two internal states. The roundabout gate, playing a pivotal role in our work, is considered in Sec. III. In Sec. IV the universal gates are physically implemented by appropriate combinations of roundabout gates, single-qubit gates, and two-particle scatterings. Section V describes how

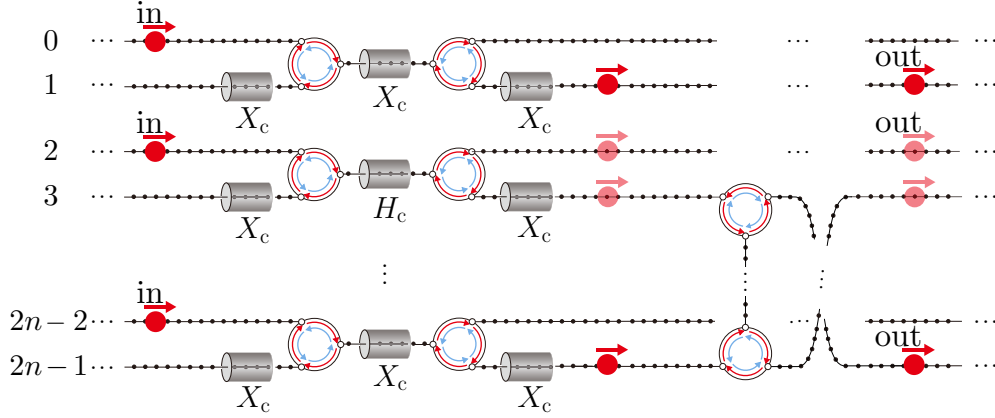


FIG. 2. Overview of our architecture for quantum computation. Initial information is represented by the positions of the quantum walkers with internal state $|0\rangle_c$ [see Eqs. (2.1) and (2.2)], which are indicated by the red walkers on the left side of the figure. The walkers (wave packets) have momenta $k \simeq -\pi/2$ and move to the right along the semi-infinite paths with group velocity $v_g = E'(-\pi/2) = 2$, where $E(k) = 2 \cos k$ [Eq. (A4)] is the energy of each walker. The quantum gates, set up like tunnels, act on the internal states of the walkers passing through them. Some pair of red walkers are scattered from each other on a vertical path connecting two paths via roundabout gates represented by (2.3) and (2.4). After the scattering, only the global phase of the two-particle wave function is changed. The position state of the quantum walkers after passing through the graph corresponds to the outcome of the computation. Note that the colors of the walkers are temporarily mixed only within single-qubit gates and are set to red otherwise. The colors do not change within the roundabout gates and during the two-particle scatterings.

to construct a practical circuit using a set of quantum gates developed in Sec. IV. Section VI is devoted to a summary. Some applications using the roundabout gate are also discussed. Technical details about scattering theory required in our paper are in the Appendix.

II. TWO-LEVEL QUANTUM WALKERS ON DIRECTED GRAPHS

A. General overview

First, let us present a general overview of our quantum computing architecture via continuous-time quantum walks with two internal states. As shown in Fig. 2, a quantum circuit is spatially designed on a graph on which multiple quantum walkers evolve continuously in time t . The dual-rail encoding is employed to represent a single-qubit state as the presence of the quantum walker in one of the two parallel paths. More specifically, a single-qubit state $|q_j\rangle$ ($q_j \in \{0, 1\}$) is given by

$$|q_j\rangle = \delta_{q_j,0}|2j\rangle_p + \delta_{q_j,1}|2j+1\rangle_p \in \mathbb{C}^2, \quad (2.1)$$

where $|j\rangle_p$ ($j \in \{0, \dots, N-1\}$) denotes the state in which a quantum walker is located on the j th path. Thus an n -qubit state $|q_{n-1} \dots q_0\rangle$ can be expressed by which of the $2n$ paths the n walkers are located on, namely,

$$|q_{n-1} \dots q_0\rangle = \bigotimes_{j=0}^{n-1} (\delta_{q_j,0}|2j\rangle_p + \delta_{q_j,1}|2j+1\rangle_p) \in (\mathbb{C}^2)^{\otimes n}. \quad (2.2)$$

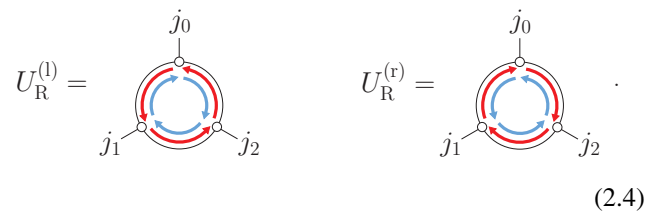
Note that here and in what follows we sometimes ignore normalization factors for simplicity of the notation. In our architecture, the quantum walkers have two internal states $|0\rangle_c \in \mathbb{C}^2$ and $|1\rangle_c \in \mathbb{C}^2$, which are normally set to $|0\rangle_c$ except during processing. For convenience, the quantum walker whose internal state is $|0\rangle_c$ ($|1\rangle_c$) is referred to as the red quantum walker (blue quantum walker).

Roughly, the computation proceeds as follows. An n -qubit input state is prepared by a position state of the red quantum walkers (see the left side in Fig. 2). Then the walkers move right along the paths, some of which are connected to roundabout gates consisting of a subgraph \hat{G}_R . The walker passing through the roundabout gate moves from one path to the next in a clockwise or counterclockwise direction, according to the internal state of the walker. Its unitary operator explicitly reads

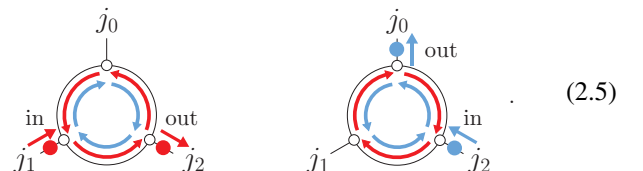
$$U_R^{(l)} = |0\rangle\langle 0|_c U_R + |1\rangle\langle 1|_c U_R^\dagger, \quad U_R^{(r)} = U_R^{(l)\dagger},$$

$$U_R = \sum_{k,l=0}^2 \delta_{l,k+1} |j_l\rangle\langle j_k|_p \quad (k, l \in \mathbb{Z}/3\mathbb{Z} = \{0, 1, 2\}), \quad (2.3)$$

where $U_R^{(l)}$ moves the red walker (blue walker) counterclockwise (clockwise) to the next path, while $U_R^{(r)}$ does the opposite to $U_R^{(l)}$. They can be graphically depicted as



For instance, the red walker (blue walker) entering the $U_R^{(l)}$ ($U_R^{(r)}$) gate from path j_1 (j_2) exits to path j_2 (j_0):



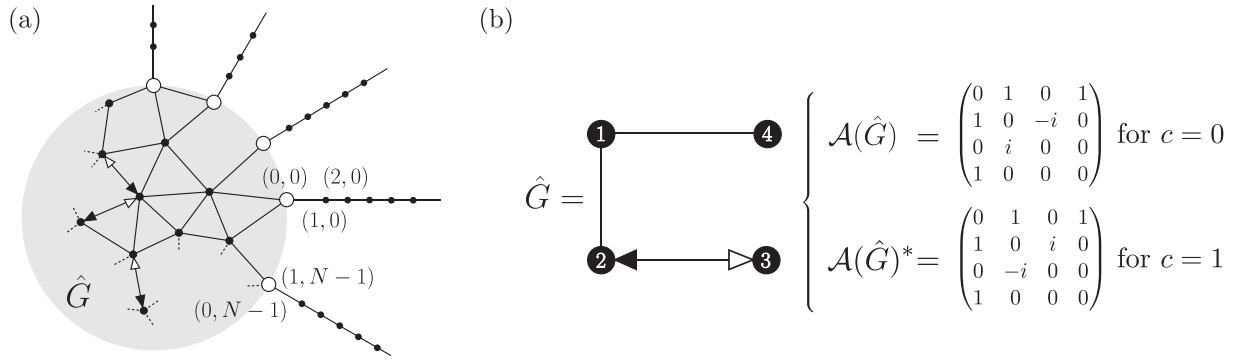


FIG. 3. (a) Schematic graph G consisting of a subgraph \hat{G} and N semi-infinite paths connected to \hat{G} (depicted on the gray disk) at the terminals denoted by the white circles. The vertices on the j th semi-infinite path are labeled by (x, j) ($x \in \mathbb{Z}_{\geq 0}$, $j \in \{0, \dots, N-1\}$). (b) Example of the directed subgraph \hat{G} and its adjacency matrix $\mathcal{A}(\hat{G})$. As shown in (2.13), in the subgraph \hat{G} , a single red walker ($c = 0$) evolves in time according to $e^{-i\mathcal{A}(\hat{G})t}$, while a blue walker ($c = 1$) evolves according to $e^{-i\mathcal{A}(\hat{G})^*t}$.

the vertex $x \in V(G)$. The operators satisfy

$$[a_{x,c}, a_{y,c'}^\dagger]_{\mp} = \delta_{x,y} \delta_{c,c'}, \quad [a_{x,c}, a_{y,c'}]_{\mp} = [a_{x,c}^\dagger, a_{y,c'}^\dagger]_{\mp} = 0, \quad (2.12)$$

where $[\cdot, \cdot]_-$ and $[\cdot, \cdot]_+$ denote the commutator for the boson operators and anticommutator for the fermion operators, respectively. The creation operators $a_{x,c}^\dagger$ generate the Hilbert space $H^{(m)}$ for m quantum walkers on G : $H^{(m)}$ is spanned by the basis vectors

$$\{|c_1 \cdots c_m\rangle_c | x_1 \cdots x_m\rangle := a_{x_m, c_m}^\dagger \cdots a_{x_1, c_1}^\dagger |0\rangle |c_1, \dots, c_m\rangle \in \{0, 1\}, x_1, \dots, x_m \in V(G)\}, \quad (2.13)$$

where $|0\rangle$ is the no-walker state (vacuum state) defined by $a_{x,c}|0\rangle = 0$ [$c \in \{0, 1\}$ and $x \in V(G)$]. The notation $|x, j\rangle$ is also used to denote the walker at (x, j) , i.e., at $x \in \mathbb{Z}_{\geq 0}$ on path j ($j \in \{0, \dots, N-1\}$). The time evolution of the m quantum walkers on the graph G is described by the action of the unitary operator $e^{-i\mathcal{H}_G t}$ on a vector in the Hilbert space $H^{(m)}$. Information about the adjacency matrix $\mathcal{A}(G) = (e^{i\theta_{xy}}) [\theta_{xy} \in \{0, \pm\pi/2\}$ and $(x, y) \in E(G)]$ of the graph G is incorporated into the kinetic term \mathcal{K}_G (2.11) as

$$\begin{aligned} (\mathcal{K}_G)_{cc', xy} &:= {}_c \langle c | \langle x | \mathcal{K}_G | c' \rangle_c | y \rangle \\ &= (e^{i\theta_{xy}} \delta_{c,0} \delta_{c',0} + e^{-i\theta_{xy}} \delta_{c,1} \delta_{c',1}) \delta_{(x,y) \in E(G)} \\ &= [\mathcal{A}(G)]_{xy} \delta_{c,0} \delta_{c',0} + [\mathcal{A}(G)^*]_{xy} \delta_{c,1} \delta_{c',1}. \end{aligned} \quad (2.14)$$

Importantly, in the directed weighted graph \hat{G} , the time evolution of a walker depends explicitly on its internal state: The evolution of a red walker (i.e., $c = 0$) is described by the unitary operator $e^{-i\mathcal{A}(\hat{G})t}$, while that of a blue walker (i.e., $c = 1$) is described by $e^{-i\mathcal{A}(\hat{G})^*t}$. [See also Fig. 3(b) for an example of \hat{G} .] It is this difference that makes the physical implementation of the roundabout gate possible. Physically, the weight $w_{xy} = e^{i\theta_{xy}}$ in (2.11) can be interpreted as a phase factor under a local gauge transformation $a_{x,c} \mapsto e^{i\theta_{x,c}} a_{x,c}$ ($\theta_{x,c} \in \mathbb{R}$), which may be achieved, for example, by applying the Aharonov-Casher effect [37,38].

Two-qubit gates are realized by taking into account two-particle scatterings of fermionic or bosonic walkers with the

same internal state. To this end, as in [23], we adopt the on-site interaction (Bose-Hubbard model) for the bosonic case and the nearest-neighbor interaction (extended Hubbard model) for the fermionic case,

$$U_G = \begin{cases} \frac{u}{2} \sum_{x \in V(G)} n_x (n_x - 1) & \text{for the bosonic walkers} \\ u \sum_{(x,y) \in E(G)} n_x n_y & \text{for the fermionic walkers,} \end{cases} \quad (2.15)$$

where $n_x := \sum_{c=0}^1 a_{x,c}^\dagger a_{x,c}$ is the number operator.

As an actual implementation, we consider a quantum walker as a wave packet $|\Psi, t\rangle = e^{-i\mathcal{H}_G t} |\Psi\rangle$ constructed by a superposition of plane waves with momentum k close to a specific value of k_p . For instance, a wave packet on a semi-infinite path (the actual implementation uses a sufficiently long path) toward a subgraph \hat{G} is given by

$$\begin{aligned} |\Psi, t\rangle &= \sum_x \frac{1}{\sqrt{2\pi}} \int_{k \simeq k_p} dk f(k) e^{-ikx - iE(k)t} |c\rangle_c |x\rangle \\ &\simeq \sum_x \frac{e^{-ik_p x - iE(k_p)t}}{\sqrt{2\pi}} \int_{k \simeq k_p} dk f(k) e^{-i(k-k_p)[x + E'(k_p)t]} |c\rangle_c |x\rangle, \end{aligned} \quad (2.16)$$

where $f(k)$ is the Fourier coefficient with a sharp peak at $k \simeq k_p$ and $E(k) = 2 \cos k$ [Eq. (A4)] is the energy of the quantum walker on the semi-infinite path. The wave packet moves with the group velocity $E'(k_p) = -2 \sin k_p$. For our purposes in the present work, we assign $k \simeq k_p = -\pi/2$ to the momentum of each walker.

Quantum computation is performed by applying unitary transformations to wave packets (2.16). What is crucial then is how to add the overall phase factor to each wave packet [note that simply translating the wave packet (2.16) as $x \mapsto x + a$ does not yield this] and how to superpose them. In our architecture, for a single quantum walker, this manipulation is essentially accomplished by unitary transformations to the internal state of the walker, and when two walkers are involved, as in controlled gates, this is accomplished by two-particle scattering. Single-particle scattering is used only for the implementation of the roundabout gate whose primary role is to

switch the position of the walker. (See Sec. IV for details.) This is in contrast to the architecture [23] where all unitary transformations are performed by single-particle and two-particle scatterings. In the Appendix we summarize single- and two-particle scatterings with a definite momentum k (i.e., scatterings of plane waves) which are key to understanding the scattering processes of wave packets with momentum close to k .

III. ROUNDABOUT GATE

The roundabout gate (2.3) or (2.4) is the most crucial element in our architecture. As schematically depicted in (2.5), the walker passing through the roundabout gate can move from one path to the next. In this section we implement the roundabout gate $U_R^{(1)}$ with single-particle scattering: We find a graph \hat{G}_R such that the S matrix $S(k)$ [$\tilde{S}(k)$] describing the scattering of the red walker (blue walker) on \hat{G}_R satisfies

$S(k) = U_R$ [$\tilde{S}(k) = U_R^\dagger$] for some specific value of k , where U_R is defined by (2.3). In fact, the scattering process only for the red walker is sufficient to study, because the S matrix $\tilde{S}(k)$ for the blue walker is nothing but the transpose of the S matrix $S(k)$ for the red walker, as shown in the Appendix [see Eq. (A9)]. Additionally, the color of the walkers does not change during the single-particle scattering, which can be seen by the Hamiltonian (2.10), especially the kinetic term (2.11). A physical implementation of another type of roundabout gate $U_R^{(r)}$ ($:=U_R^{(1)\dagger}$) in (2.3) can be easily accomplished by replacing the subgraph \hat{G}_R with \hat{G}_R^* whose adjacency matrix is given by $\mathcal{A}(\hat{G}_R^*) = \mathcal{A}(\hat{G}_R)^*$.

The S matrix $S(k)$ of the red walker characterizing the scattering state is expressed in terms of the elements of the adjacency matrix $\mathcal{A}(\hat{G}_R)$, as shown in (A7), which serves as a clue to find the desired adjacency matrix. (See the Appendix for scattering theory required in this section.) Using (A7), we find that the three graphs

$$\hat{G}_R^{(1)} = \quad \hat{G}_R^{(2)} = \quad \hat{G}_R^{(3)} = \quad (3.1)$$

with the abbreviation of the directed weighted edge

$$\mathcal{A}(\textcircled{1} \leftarrow \textcircled{2}) := \begin{pmatrix} 0 & -i \\ i & 0 \end{pmatrix}, \quad \mathcal{A}(\textcircled{1} \leftarrow \textcircled{2})^* := \mathcal{A}(\textcircled{1} \rightarrow \textcircled{2}) = \begin{pmatrix} 0 & -i \\ i & 0 \end{pmatrix} \quad (3.2)$$

all implement the roundabout gate up to the sign (the minus sign is necessary for $\hat{G}_R^{(1)}$), when the momentum of the walker passing through them is exactly $k = -\pi/2$: $S(-\pi/2) = U_R$ for the red walker and $\tilde{S}(-\pi/2) = S(-\pi/2)^T = U_R^\dagger$ [cf. (A9)] for the blue walker. More explicitly, the matrix elements of $S(k) = \sum_{m,n} S_{mn}(k)|0, m\rangle\langle 0, n|$ are given by

$$S_{00}(k) = \frac{-e^{Aik}}{1 + 2i \tan k}, \quad S_{10}(k) = \frac{-2e^{7ik/2 - i\pi/4} \cos\left(\frac{k}{2} + \frac{\pi}{4}\right)}{2 - i \cot k}, \quad S_{20}(k) = \frac{-2ie^{7ik/2 - i\pi/4} \sin\left(\frac{k}{2} + \frac{\pi}{4}\right)}{2 - i \cot k},$$

$$S_{11}(k) = S_{00}(k), \quad S_{21}(k) = S_{10}(k), \quad S_{22}(k) = S_{00}(k) \quad (3.3)$$

for $\hat{G}_R^{(1)}$ and

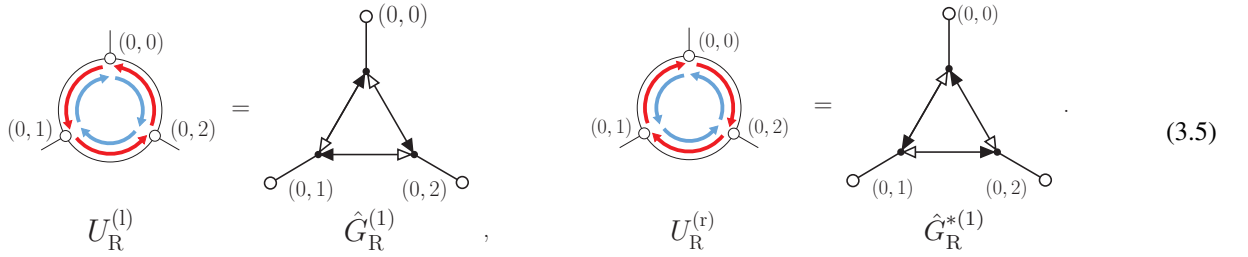
$$S_{00}(k) = \frac{-e^{Aik}}{1 + 2i \tan k}, \quad S_{10}(k) = \frac{2e^{7ik/2 - i\pi/4} \cos\left(\frac{k}{2} + \frac{\pi}{4}\right)}{2 - i \cot k}, \quad S_{20}(k) = \frac{2e^{9ik/2 - i\pi/4} \sin\left(\frac{k}{2} + \frac{\pi}{4}\right)}{2 - i \cot k},$$

$$S_{11}(k) = S_{00}(k), \quad S_{21}(k) = \frac{2e^{9ik/2 + i\pi/4} \cos\left(\frac{k}{2} + \frac{\pi}{4}\right)}{2 - i \cot(k)}, \quad S_{22}(k) = e^{2ik} S_{00}(k) \quad (3.4)$$

for $\hat{G}_R^{(2)}$ and $\hat{G}_R^{(3)}$. The other elements are determined by the relation $S(k) = S(-k)^\dagger$, which holds for $k \in \mathbb{R}$ [see Eq. (A8)].

The probability that a walker entering \hat{G}_R from path $m \in \mathbb{Z}/3\mathbb{Z} = \{0, 1, 2\}$ will be found on path $n \in \mathbb{Z}/3\mathbb{Z} = \{0, 1, 2\}$ is given by $|S_{mn}(k)|^2$, which is the same for all three cases in (3.1). We see that the walker with momentum $k = -\pi/2$ perfectly transmits from n to $m = n + 1$. In Fig. 4 the momentum dependence of the transmission probabilities is shown. In summary, the subgraphs $\hat{G}_R^{(j)}$ and $\hat{G}_R^{*(j)}$ ($j = 1, 2, 3$) are physical implementations of the roundabout gates $U_R^{(1)}$ and $U_R^{(r)}$, respectively, for a

quantum walker with momentum $k = -\pi/2$. Graphically,



The same is true for $G_R^{(j)}$ and $G_R^{*(j)}$ ($j = 2, 3$) as shown above. Note that \hat{G}_R^* is obtained by reversing all the arrows in \hat{G}_R [Eq. (3.1)], because $\mathcal{A}(\hat{G}_R^*) = \mathcal{A}(\hat{G}_R)^*$.

In the actual implementation, we use a wave packet (2.16) as a quantum walker and consider the scattering state on the subgraph \hat{G}_R with sufficiently long (but finite length) paths attached. The effective length of the subgraph \hat{G}_R can be evaluated by the nontrivial phase shift of the wave packet output from \hat{G}_R after scattering. The wave packet $|\Psi_{\text{out}}, t\rangle$ for the red walker exiting from $(0, l)$, which entered \hat{G}_R from $(0, j)$ [cf. (A1) and (2.16)], is given by

$$\begin{aligned} |\Psi_{\text{out}}, t\rangle &= \frac{1}{\sqrt{2\pi}} \int_{k \geq k_p} dk S_{lj}(k) f(k) e^{ikx - iE(k)t} |0\rangle_c |x\rangle \\ &\simeq \frac{S_{lj}(k_p) e^{ik_p x - iE(k_p)t}}{\sqrt{2\pi}} \\ &\quad \times \int_{k \geq k_p} dk f(k) e^{i(k-k_p)[x - i(\ln S_{lj})'(k_p) - E'(k_p)t]} |0\rangle_c |x\rangle. \end{aligned} \quad (3.6)$$

Thus, the effective length

$$\ell_{lj}(k) := -i(\ln S_{lj})'(k) \quad (3.7)$$

for the red walker is calculated by (3.3) or (3.4),

$$\begin{aligned} \ell_{lj}\left(-\frac{\pi}{2}\right) &= 3\delta_{l,j+1} \text{ for } G_R^{(1)}, \\ \ell_{lj}\left(-\frac{\pi}{2}\right) &= \begin{cases} 3\delta_{l,j+1} & \text{for } j = 0 \\ 4\delta_{l,j+1} & \text{for } j = 1, 2 \end{cases} \text{ for } G_R^{(2)} \text{ and } G_R^{(3)}, \end{aligned} \quad (3.8)$$

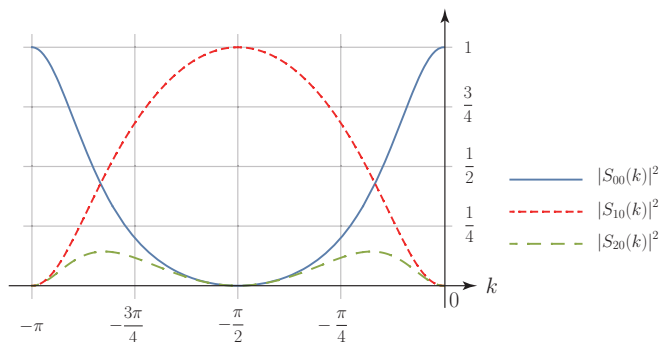


FIG. 4. Momentum dependence of the probability $|S_{m0}(k)|^2$ ($m = 0, 1, 2$) that a walker entering $\hat{G}_R^{(j)}$ ($j \in \{1, 2, 3\}$) (3.1) from path 0 will be found on path m ($m = 0, 1, 2$). The walker with momentum $k = -\pi/2$ completely transmits from path 0 to path 1.

where $j, l \in \mathbb{Z}/3\mathbb{Z} = \{0, 1, 2\}$. On the other hand, the effective length $\tilde{\ell}_{lj}(k)$ for the blue walker is given by the relation

$$\tilde{\ell}_{lj}(k) = \ell_{jl}(k) \quad (k \in \mathbb{R}), \quad (3.9)$$

which follows from (A9). These effective lengths are necessary for building actual finite-size quantum circuits, where a synchronization of the motion of quantum walkers becomes crucial. (See Sec. V for details.)

IV. ELEMENTARY QUANTUM GATES

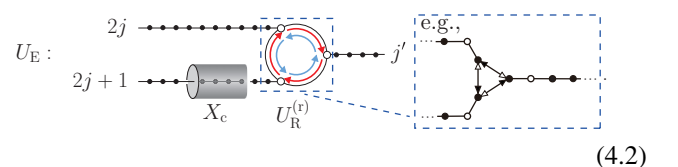
In this section we describe how to implement a universal quantum gate set via two-level quantum walkers. As described in Sec. II, information is spatially encoded by the positions of red quantum walkers. Information processing is carried out by moving multiple quantum walkers to appropriate positions. In our architecture, the internal state of the quantum walker serves as a temporal storage medium during this process. Any unitary transformation to a single-qubit state can be replaced by a transformation to the internal state of the quantum walker. There the roundabout gate not only switches the position of the walkers but acts as an information encoder and decoder. In addition, combining two-particle scattering on an infinite path, one can implement a controlled gate.

A. Single-qubit gates

First, let us implement a unitary operator U acting on a single-qubit state $|q_j\rangle$ defined as (2.1). In our scheme, we express the state as the position of the red quantum walker:

$$|0\rangle_c |q_j\rangle = |0\rangle_c |2j + q_j\rangle_p \in \mathbb{C}^2 \otimes \mathbb{C}^2. \quad (4.1)$$

The information $|q_j\rangle$ can be encoded into the internal state of the walker passing through the following encoder U_E , which consists of the Pauli X gate X_c [Eq. (2.7)] and the roundabout gate $U_R^{(r)}$ [Eq. (2.4)]:



Let us explain in detail. A red walker prepared on the $(2j)$ th or $(2j + 1)$ th input path (possibly in superposition) moves

toward the roundabout gate $U_R^{(r)}$; the red walker on the $(2j+1)$ th path changes color to blue at the X_c gate before entering $U_R^{(r)}$. The roundabout gate $U_R^{(r)}$ consists of the subgraph \hat{G}_R^* moving the red walker (blue walker) clockwise (counterclockwise) to output path j' , as shown in the preceding section. For example, the inset depicts $\hat{G}_R^{*(1)}$ [cf. (3.5)]. The effective length of $U_R^{(r)}$ can be exactly the same for the red and blue walkers, if the terminal vertices $(0, j)$ ($j \in \{0, 1, 2\}$) of \hat{G}_R^* as in (3.5) and (3.1) are connected to paths $\{2j, 2j+1, j'\}$ in (4.2) so that $(0, 0) \rightarrow (0, 2j)$, $(0, 1) \rightarrow (0, 2j+1)$, and $(0, 2) \rightarrow (0, j')$. More precisely, one finds

$$\ell_{j', 2j} \left(-\frac{\pi}{2} \right) = \tilde{\ell}_{j', 2j+1} \left(-\frac{\pi}{2} \right) = \begin{cases} 3 & \text{for } \hat{G}_R^{*(1)} \\ 4 & \text{for } \hat{G}_R^{*(2)}, \hat{G}_R^{*(3)}, \end{cases} \quad (4.3)$$

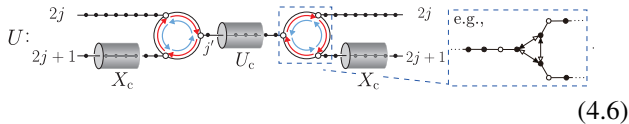
where $\ell_{j', 2j}(-\pi/2)$ and $\tilde{\ell}_{j', 2j+1}(-\pi/2)$ are the effective lengths of $U_R^{(r)}$ for the red and blue walkers, respectively. This is derived from (3.8), (3.9), and the fact that the S matrix for \hat{G}_R^* is given by the transpose of that for \hat{G}_R , as shown in (A9). Equation (4.2) equivalently reads

$$(4.1) \xrightarrow{X_c \otimes (|2j+1\rangle\langle 2j+1|)_p} \delta_{q_j, 0} |0\rangle_c |2j\rangle_p + \delta_{q_j, 1} |1\rangle_c |2j+1\rangle_p \xrightarrow{U_R^{(r)}} |q_j\rangle_c |j'\rangle_p. \quad (4.4)$$

Applying a unitary gate U_c to the internal state of the walker moving in the right direction on path j' and then applying the decoder U_D [Eq. (2.8)] realized by the reverse operation of the encoder U_E [Eq. (4.2)] (i.e., $U_D = U_E^\dagger$), we obtain the desired state $U|q_j\rangle$:

$$(4.4) \xrightarrow{U_c} (U_c |q_j\rangle_c) |j'\rangle_p \xrightarrow{U_D = U_E^\dagger} |0\rangle_c (U|q_j\rangle). \quad (4.5)$$

Graphically, the single-qubit gate is depicted as



It is known [39,40] that any single-qubit unitary gate U is realized by

$$U = e^{i\theta_0} R_z(\theta_1) R_y(\theta_2) R_z(\theta_3) \quad (\theta_j \in \mathbb{R}), \quad (4.7)$$

where

$$R_y(\theta) := \exp\left(-i\frac{\theta Y}{2}\right), \quad R_z(\theta) := \exp\left(-i\frac{\theta Z}{2}\right) \quad (4.8)$$

are the rotation operators about y and z axes of the Bloch sphere, respectively; Y and Z are the Pauli matrices σ_y and σ_z , respectively. Actually, for instance, in the spin-1/2 fermionic system, the rotation gates acting on the spin state may be implemented by applying a uniform magnetic field H in a particular direction over a suitable interval of the path. See Fig. 5 for a schematic description of a rotation gate $R_y(\theta)_c$ acting on the internal state of the walker. Since the Zeeman energy \mathcal{H}_{ex} is given by $\mathcal{H}_{\text{ex}} = HY/2$ ($\mathcal{H}_{\text{ex}} = HZ/2$) for the magnetic field H applied in the negative direction of the y axis (z axis), the spin state of the walker passing through the device over time t is transformed by the operator $R_y(Ht)_c = e^{-itHY_c/2}$

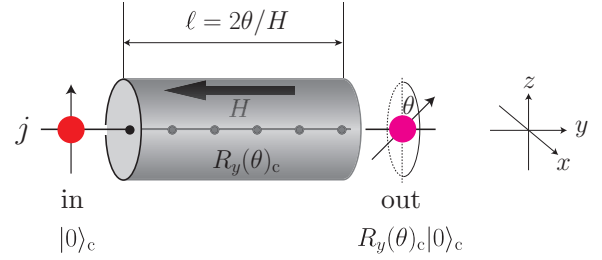


FIG. 5. Schematic description of the rotation gate $R_y(\theta)_c$ for the spin-1/2 fermionic system. A uniform magnetic field H is applied in the negative direction of the y axis in the device set up like tunnels along the path. Since the speed of the walker is $v_g = 2$ [Eq. (4.9)] and the Zeeman energy $\mathcal{H}_{\text{ex}} = H\sigma_y/2 = HY/2$, $R_y(\theta)_c = e^{-i\theta Y_c/2}$ is implemented by just setting the length of the device to $\ell = 2\theta/H$.

$[R_z(Ht)_c = e^{-itHZ_c/2}]$. Because the (group) velocity v_g of the quantum walker with momentum $k = -\pi/2$ is

$$v_g = E' \left(-\frac{\pi}{2} \right) = -2 \sin \left(-\frac{\pi}{2} \right) = 2 \quad (4.9)$$

[see Eq. (A4)], $R_{y,z}(\theta)_c$ can be implemented by just setting the device length ℓ so that $\theta = tH = \ell H/v_g$, i.e., $\ell = 2\theta/H$.

B. Two-qubit gates

Appropriately combining the scattering of two walkers with the same internal state and a single-qubit gate described above, we can implement a two-qubit gate. The aforementioned single-qubit rotation gates and a controlled-NOT (CNOT) gate are elements of a universal gate set [39,40]. In fact, the CNOT gate $\text{CNOT}_{j_0 j_1}$ acting on a two-qubit state $|q_{j_1}\rangle|q_{j_0}\rangle$ is decomposed into

$$\text{CNOT}_{j_0 j_1} = H_{j_1} \text{CP}_{j_0 j_1}^2 H_{j_1}, \quad (4.10)$$

where H_{j_1} is the Hadamard gate on $|q_{j_1}\rangle$ and $\text{CP}_{j_0 j_1}$ is a controlled-phase gate on $|q_{j_1}\rangle|q_{j_0}\rangle$:

$$\text{CP} = \begin{pmatrix} 1 & 0 & 0 & 0 \\ 0 & 1 & 0 & 0 \\ 0 & 0 & 1 & 0 \\ 0 & 0 & 0 & \pm i \end{pmatrix}. \quad (4.11)$$

As explained earlier, the action of H_{j_1} can be replaced by the action on the internal state of the quantum walker moving along path j'_1 , which is connected to paths $2j_1$ and $2j_1+1$ by roundabout gates. The CP gate, on the other hand, is implemented by two-particle scattering on an infinite path: Two particles, moving along paths $2j_0+1$ and $2j_1+1$, respectively, are switched by the roundabout gate to the same infinite path and travel toward each other with momenta $k_0 = -\pi/2$ and $k_1 = \pi/2$ to be scattered from each other. Due to the conservation laws of energy and momentum, the individual momenta are also conserved after scattering. As a result, only the global phase of the two-particle wave function can be changed. In the Appendix we evaluate the phase for both the bosonic and fermionic cases. For the bosonic system with $u = \mp 4$ in the interaction term (2.15), the wave function acquires a phase $S_{01}(k_0 = -\pi/2, k_1 = \pi/2) = \pm i$ after scattering [see (A15)]. For the fermionic case, a global phase $S_{01}(k_0 = -\pi/2, k_1 = \pi/2) = \pm i$ is acquired for $u = \mp 2$. Consequently, the CP gate is implemented by two

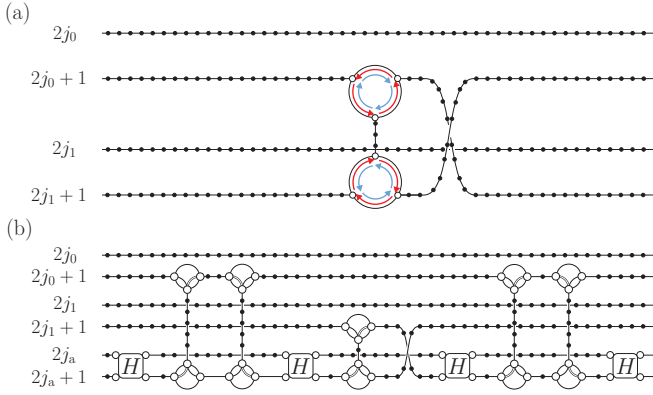


FIG. 6. (a) Controlled-phase gate (4.11) implemented in the present model. (b) Controlled-phase gate implemented in the model [23]. In contrast to (b), single-particle scattering is used in (a) only for the implementation of the roundabout gate. Since (a) does not require ancilla qubits [corresponding to \$|2j_a\rangle_p\$ and \$|2j_a + 1\rangle_p\$ in (b)], the architecture can be drastically simplified compared to (b).

roundabout gates as depicted in Fig. 6. Characteristically, our architecture does not require any ancilla qubit; therefore, the structure of controlled gates can be significantly simplified, compared to those in [23]. Finally, we graphically represent the CNOT gate (4.10) in Fig. 7.

In the actual implementation of the two-qubit gates, we use wave packets (2.16) as quantum walkers and consider the scattering state on a sufficiently long (but finite length) paths. The effective length \$\ell(-\pi/2)\$ for each walker in the two-particle scattering is obtained via (A11), (A15), and (A18):

$$\begin{aligned} \ell\left(-\frac{\pi}{2}\right) &= -i\partial_{k_0} \ln S\left(k_0 = -\frac{\pi}{2}, k_1 = \frac{\pi}{2}\right) \\ &= i\partial_{k_1} \ln S\left(k_0 = -\frac{\pi}{2}, k_1 = \frac{\pi}{2}\right) \\ &= \begin{cases} 0 & \text{for bosons} \\ -1/2 & \text{for fermions.} \end{cases} \end{aligned} \quad (4.12)$$

Finally, we would like to comment on the reversibility of our architecture. Since the adjacency matrix of the graph used in the current architecture is a Hermitian matrix, the time evolution of the quantum walkers is of course described by a unitary operator. In this sense, quantum computation using the present model is as reversible as ordinary quantum computers. However, simply reversing the motions of the walkers on the output paths (i.e., giving them the opposite momenta) is not enough to return them to their initial positions on the input paths. To return them to their original positions, one must not only reverse the motions of the walkers, but also replace the clockwise roundabout gates with counterclockwise roundabout gates and vice versa. Alternatively, we can also return them to the original positions by changing the colors of the walkers on the output paths from red (spin-up) to blue (spin-down), reversing the direction of all the magnetic fields applied in the single-qubit devices (see Fig. 5), and reversing the motions of the walkers (i.e., time-reversal symmetry).

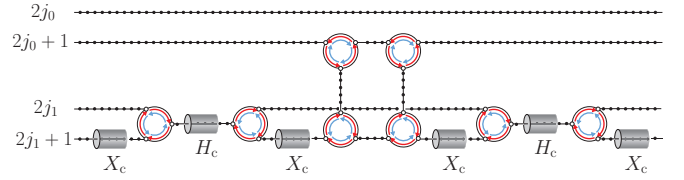


FIG. 7. Graphical representation of the CNOT gate (4.10).

V. BUILDING A CIRCUIT

The quantum walker is effectively realized by a wave packet consisting of plane waves with momentum close to a specific value of \$k \simeq k_p\$ [see (2.16), for instance]. As explained earlier, in our architecture, \$k_p = -\pi/2\$ is assigned to design quantum gates. To build a quantum circuit for practical use, we must truncate the semi-infinite paths connected to each subgraph and consider scatterings of wave packets on a finite-size graph (circuit). There the timing of the two-particle scatterings becomes crucial: The two-particle scatterings must occur at the proper vertical paths. Here we explain how to arrange the quantum gates to build a practical circuit, according to the procedure developed in [23]. Also an error bound is estimated. Let us build an \$n\$-qubit circuit. Any quantum circuit can be designed by appropriately combining blocks consisting of single-qubit gates (type 1 blocks) and blocks consisting of CP gates (type 2 blocks), as depicted in Fig. 8. The input and output \$n\$-qubit state \$|q_{n-1} \dots q_0\rangle\$ (\$q_j \in \{0, 1\}\$, \$j \in \{0, \dots, n-1\}\$) of each block is dual-rail encoded by \$n\$ red quantum walkers [cf. (4.1)], given by the wave packet of length \$L\$,

$$|q_j\rangle = \frac{1}{\sqrt{L}} \sum_{x=L}^{2L-1} e^{\pm i(\pi/2)x} |0\rangle_c |x, 2j + q_j\rangle_{in(out)}, \quad (5.1)$$

where \$|x, j\rangle_{in(out)}\$ denotes the position state of a particle on the \$j\$th input (output) path and the positive and negative signs in the exponential correspond to the input and output wave packets, respectively. Also, the length of each input and output path connecting to each block is set to \$3L\$ and the output paths of one block are commonly used as the input paths for the subsequent block. The state (5.1) is expressed as the wave packet located in the center of each path. Incidentally, the input wave packet (5.1) itself is given by the superposition of plane waves (2.16) with the probability amplitude

$$f(k) = \sqrt{\frac{2}{L\pi}} \frac{\sin\left[\frac{L-1}{2}\left(k + \frac{\pi}{2}\right)\right]}{k + \frac{\pi}{2}} e^{(3L-1)/2(k+\pi/2)i}. \quad (5.2)$$

Now let us consider how the quantum gates in blocks of type 1 and type 2 can be arranged so that the desired pair of red walkers can meet simultaneously on a particular vertical path. As shown in Fig. 8, a block of type 1 consists of \$n\$ single-qubit gates \$U_0, \dots, U_{n-1}\$ (some of which may be identity gates), in which \$(U_j)_c\$ acts on the internal state of the walker transferred from path \$2j\$ or \$2j + 1\$ by the leftmost roundabout gate. As explained in Sec. IV, it is possible to make the effective lengths of the roundabout gates for the red and blue walkers exactly the same by incorporating the graphs \$\hat{G}_R\$ and \$\hat{G}_R^*\$ in the proper orientation. If the quantum gates are assembled in

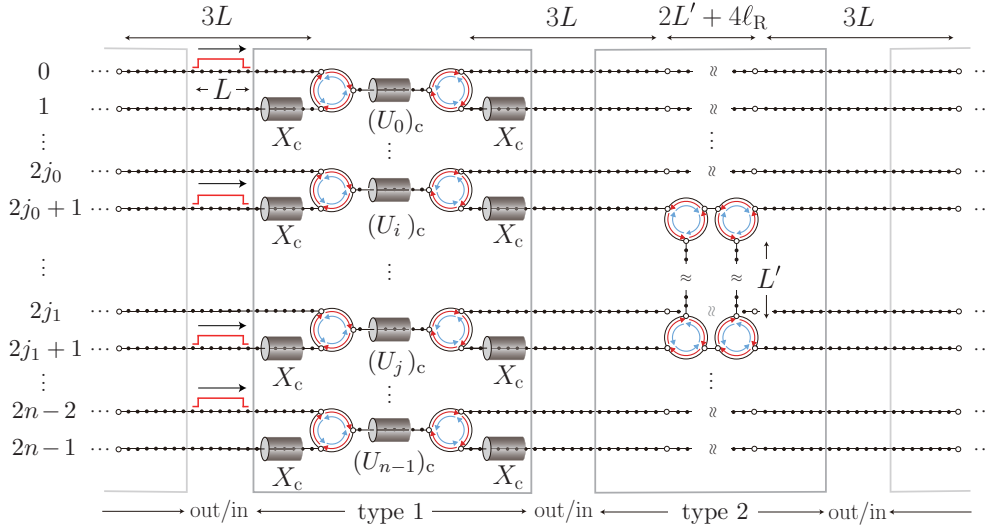


FIG. 8. In the actual n -qubit circuit, n wave packets of length L are employed as quantum walkers to represent an n -qubit state. Any circuit can be built by a proper combination of type 1 and type 2 blocks. A block of type 1 consists of n single-qubit gates U_0, \dots, U_{n-1} (some of which may be identity gates). A block of type 2 consists of a set of CP gates $CP_{j_0 j_1}$ ($j_0 \neq j_1$, $j_0, j_1 \in \{0, \dots, n-1\}$) constructed by four roundabout gates. An identity gate in a block of type 2 is realized by simply connecting the input and output of the block with a straight path of length $2L' + 4\ell_R$, where $L' \geq 4L$ is the length of each vertical path connecting the upper and lower two roundabout gates within each CP gate and ℓ_R is the effective length of the roundabout gate [see Eq. (3.8)]. Input and output paths of length $3L$ each are attached to each block, where the output paths of one block are commonly used as the subsequent block.

such a manner, quantum walkers that simultaneously enter a block of type 1 will exit that block at the same time. In other words, type 1 blocks do not affect the order of walkers.

A block of type 2 consists of a set of CP gates $CP_{j_0 j_1}$ ($j_0 \neq j_1$ and $j_0, j_1 \in \{0, \dots, n-1\}$) and identity gates. In contrast to a block of type 1, an identity gate is realized by simply connecting the input and output with a straight path. As a CP gate, we employ

$$CP_{j_0 j_1} = \begin{pmatrix} 1 & 0 & 0 & 0 \\ 0 & 1 & 0 & 0 \\ 0 & 0 & 1 & 0 \\ 0 & 0 & 0 & -1 \end{pmatrix}_{j_0 j_1} \quad (5.3)$$

instead of (4.11), taking into account the effective length (4.12) of the two-particle scattering of fermionic walkers. This CP gate is achieved by placing four roundabout gates as shown in Fig. 8. The right terminal vertex on path $2j_0 + 1$ or $2j_1 + 1$ of the left roundabout gate can be directly connected to the right terminal vertex of the right roundabout gate without compromising the function of the gate. Let us set the length of each vertical path to $L' \geq 4L$ and denote the effective length of each roundabout gate by ℓ_R [i.e., $\ell_R = 3$ or 4 from (3.8)]. Then if we set the length of the straight path of the identity gate to $2L' + 4\ell_R$, a particular pair of red walkers simultaneously entering the block can be scattered within a specific vertical path. In addition, for the fermionic walks, we must take into account the effective length (4.12) of the two-particle scattering: The scattered fermionic walkers in the CP gate move ahead of other walkers by one vertex. In this case, by increasing the number of vertices in each horizontal and vertical path by one in the next type 2 block, the desired two-particle scattering can occur within a specific vertical path in the next block. Namely, in the m th type 2 block, the

number of vertices in each horizontal and vertical path should be increased by m more than in the first.

As explained in Secs. III and IV, the roundabout gate and the CP gate are designed based on single- and two-particle scattering states of plane waves with a definite momentum $k = k_p$, which are defined on the subgraph with a semi-infinite path and on the straight vertical path of infinite length, respectively. Therefore, to ensure the reliability of the architecture, it is also essential to estimate errors that occur in an actual quantum circuit consisting of a finite-size graph on which the wave packets move as quantum walkers. Let $|\Psi_{\text{in}}\rangle$ be an input state in superposition [cf. (5.1)],

$$|\Psi_{\text{in}}\rangle = \frac{1}{\sqrt{L}} \sum_{\{q_j\}} \bigotimes_{j=0}^{n-1} \left(\sum_{x=L}^{2L-1} e^{i(\pi/2)x} |0\rangle_c |x, 2j + q_j\rangle_{\text{in}} \right), \quad (5.4)$$

and $e^{-i\mathcal{H}_{\text{tot}}\tau} |\Psi_{\text{in}}\rangle$ be the output state after processing over time τ in a circuit intended to implement a unitary operator U , where \mathcal{H}_{tot} is the total Hamiltonian for the circuit, consisting of the kinetic term (2.11), interaction term (2.15), and Zeeman energies used in the single-qubit gates (see Sec. IV). An error bound between the desired state $|\Psi_{\text{out}}\rangle$,

$$|\Psi_{\text{out}}\rangle = \frac{1}{\sqrt{L}} \sum_{\{q_j\}, \{q'_j\}} \langle q'_{n-1} \cdots q'_0 | U | q_{n-1} \cdots q_0 \rangle \bigotimes_{j=0}^{n-1} \left(\sum_{x=L}^{2L-1} e^{-i\frac{\pi}{2}x} |0\rangle_c |x, 2j + q'_j\rangle_{\text{out}} \right), \quad (5.5)$$

and the actual output state $e^{-i\mathcal{H}_{\text{tot}}\tau} |\Psi_{\text{in}}\rangle$ is estimated by directly applying the method in [23] (see also [41]). It yields

$$\| |\Psi_{\text{out}}\rangle - e^{-i\mathcal{H}_{\text{tot}}\tau} |\Psi_{\text{in}}\rangle \| = O(gn^3 L^{-1/4}), \quad (5.6)$$

where g is the total number of type 1 and type 2 blocks. This error bound is obtained by multiplying an error bound $O(gnL^{-1/4})$ due to the use of wave packets by an error bound $O(n^2)$ due to truncation of the semi-infinite paths in each block [23]. Note that errors in the gates acting on the internal states $|c\rangle_c$ can be neglected for the following reasons. These gates, for instance, X_c and H_c as in (2.6) or (2.7), are designed for a wave packet with group velocity $v_g = 2$ (see Fig. 5). Errors in these gates mainly come from a distortion of the wave packet by higher-order dispersion effect: The velocity of the wave packet is corrected as

$$v \simeq E'(k_p) + \frac{1}{2}(k - k_p)E''(k_p) + \frac{1}{6}(k - k_p)^2 E'''(k_p) = v_g + O\left(\frac{1}{L^2}\right), \quad (5.7)$$

where we have used $k_p = -\pi/2$, $E(k) = 2 \cos k$, and also $|k - k_p| = O(1/L)$, which follows from (5.2). Thus, the error caused by the correction (5.7) is estimated to be $O(nL^{-2})$ at each block, which is negligible compared to the above error bound $O(nL^{-1/4})$ due to scatterings of wave packets.

As pointed out in [23], the error bound estimated in (5.6) is almost surely not optimal; a significant improvement can be expected. Nevertheless, by setting $L = O(g^4 n^{12})$, one finds that universal quantum computation of arbitrary precision can be achieved with polynomial overhead. Namely, the total number of vertices in the architecture is $O(g^5 n^{13})$ and the total computational time is $O(g^5 n^{12})$, which are formally the same as the architecture in [23]. However, a feature of our architecture is that the number of blocks g can be significantly reduced by using $O(ng)$ gates acting on the internal states, as shown in Fig. 6, which is expected to enable more efficient implementation for universal computation than in [23].

VI. SUMMARY AND DISCUSSION

We have proposed a model of universal quantum computing using a multiparticle continuous-time quantum walk. Quantum information is dual-rail encoded by the quantum walkers with two internal states (colors) $|0\rangle_c$ (red) and $|1\rangle_c$ (blue). To process the information spatially, we have newly developed the roundabout gate that moves the quantum walker from one path to the next, clockwise or counterclockwise, depending on the color of the quantum walker. Any single-qubit unitary transformation is converted to a transformation for the color of the quantum walker. In this transformation, the roundabout gate acts as an information encoder and decoder. Two quantum walkers can be scattered from each other on an infinite path to change a global phase of the two-particle wave function. An appropriate combination of a single-qubit gate and two-particle scattering yields a two-qubit controlled gate.

Our approach has several advantages. (i) Two-level quantum walkers can be realized with very mundane particles such as electrons and spin-1 bosons. The Bose-Hubbard model (bosonic walks) and the extended Hubbard model (fermionic walks) employed in the architecture are models commonly used in many-particle physics. (ii) Simplification of design is possible. The single-particle scattering is only applied to implement the roundabout gate. Instead, a single-qubit gate is realized by a quantum device that acts on the color of the

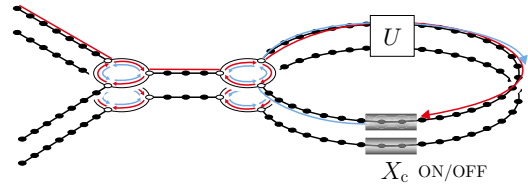


FIG. 9. Example of a circuit that serves as a quantum memory. Information can be stored and retrieved at will by switching on the Pauli X gates installed on the loop. Iterative calculations can also be easily carried out by simply placing unitary gates on the loop, which may be helpful to perform, for instance, the Grover algorithm.

quantum walker. The subgraph \hat{G}_R for the roundabout gate can be designed to be as simple as possible: The total number of vertices is at most 7, the maximum degree of \hat{G} is 3, and the edge weights of the graph take only 1 and $\pm i$ [see (3.1) and (3.5)]. The colors of the walker coexist temporarily within the individual single-qubit gates. In other words, maintaining the coherence of the colors is only required within individual single-qubit gates. The two-particle scattering necessary to realize a two-qubit gate occurs only between a pair of red walkers and only in a straight path. For the implementation, any ancilla qubit is unnecessary. (iii) An automatic quantum computation is possible: The computation is done by just passing quantum walkers through appropriately designed paths. (iv) A unified design of quantum computing compatible with an automatic QRAM is possible.

Here we would like to discuss some possible applications using our architecture. A crucial and nontrivial application is a physical realization of a QRAM, as briefly introduced in the Introduction and above. The details will be proposed in the following paper [35]. Some simple quantum memory can also be constructed by a suitable combination of the roundabout gate, as in Fig. 9. The quantum walkers, which represent the result of the calculation, can be led into the loops by the roundabout gates and stored as information. The information can be freely retrieved by switching on the Pauli X gates installed on the loops. Iterative calculations can also be easily carried out by simply placing unitary gates on the loop. It might be helpful to efficiently perform information processing such as the Grover search [42], the quantum phase estimation [43], and the quantum version of fast Fourier transform [44].

The roundabout gate is essential in the present architecture and automatic QRAM. Theoretically, this can be realized by imposing an internal-state-dependent gauge factor as shown in (2.11). Experimentally, it may be possible to achieve this, e.g., by applying the Aharonov-Casher effect [37,38], but this still remains open.

ACKNOWLEDGMENT

The present work was partially supported by Grant-in-Aid for Scientific Research (C) No. 20K03793 from the Japan Society for the Promotion of Science.

APPENDIX: SINGLE- AND TWO-PARTICLE SCATTERING

In this Appendix, to make our paper self-contained, we summarize single- and two-particle scattering states of indistinguishable quantum walkers.

1. Single-particle scattering on a graph

First, we consider the single-particle scattering on the graph G defined in Fig. 3, using the procedure introduced in [23,36]. Since the color of a single walker does not change [see (2.11)], the single-particle scattering can be considered independently in the case of a red walker and a blue walker. Therefore, first, we fix the color of the walker to red ($c = 0$) [correspondingly, we only consider the part of $c = 0$ in the kinetic term (2.11)] and omit the internal state $|0\rangle_c$ to simplify the notation. Later we will show that the single-particle S matrix of the blue walker is nothing but the transpose of that for the red walker.

Consider the process in which an incident walker (wave packet) with a momentum near a specific value of $k \in (-\pi, 0)$ passes through the j th semi-infinite path toward the graph \hat{G} and exits to some semi-infinite paths l (in superposition) after scattering from \hat{G} . Since an arbitrary wave packet is given by the superposition of plane waves of momentum close to k as in (2.16), the scattering state $|\varphi_j(k)\rangle$ with a definite k gives us information about how the wave packet scatters from \hat{G} . It is generally written as

$$|\varphi_j(k)\rangle = \sum_{x=0}^{\infty} e^{-ikx} |x, j\rangle + \sum_{l=0}^{N-1} \sum_{x=0}^{\infty} S_{lj}(k) e^{ikx} |x, l\rangle + \sum_{x \in V(\hat{G}) \setminus T} \psi_j(x; k) |x\rangle, \quad (\text{A1})$$

where $|x, j\rangle$ denotes a walker at x on the j th semi-infinite path [i.e., the walker at (x, j)], $V(\hat{G}) \setminus T$ is the set of the M internal vertices of \hat{G} , $S_{lj}(k) \in \mathbb{C}$ is the element of the S matrix, and $\psi_j(x; k) \in \mathbb{C}$ is the wave function on \hat{G} , which can be determined by the Schrödinger equation

$$\langle x | \mathcal{K}_G | \varphi_j(k) \rangle = E(k) \langle x | \varphi_j(k) \rangle \quad [x \in V(G)]. \quad (\text{A2})$$

Here \mathcal{K}_G is the kinetic term defined as (2.11). Note that the interaction term (2.15) does not contribute to the single-particle scattering and the color of the walker is implicitly assumed to be red ($|0\rangle_c$), as explained above. In particular, for (x, l) ($x \geq 1$), we have

$$\langle x, l | \mathcal{K}_G | \varphi_j(k) \rangle = 2 \cos k \langle x, l | \varphi_j(k) \rangle, \quad \langle x, l | \varphi_j(k) \rangle = e^{-ikx} \delta_{l,j} + e^{ikx} S_{lj}(k), \quad (\text{A3})$$

which determines the energy $E(k)$:

$$E(k) = 2 \cos k. \quad (\text{A4})$$

On the other hand, the Schrödinger equation (A2) for $x \in \hat{G}$ is written as

$$\begin{pmatrix} A & B^\dagger \\ B & D \end{pmatrix} \begin{pmatrix} I_N + S(k) \\ \psi(k) \end{pmatrix} + \begin{pmatrix} e^{-ik} I_N + e^{ik} S(k) \\ 0 \end{pmatrix} = E(k) \begin{pmatrix} I_N + S(k) \\ \psi(k) \end{pmatrix}, \quad (\text{A5})$$

where

$$S(k) := \sum_{l=0}^{N-1} \sum_{j=0}^{N-1} S_{lj}(k) |0, l\rangle \langle 0, j| \in \text{End}(\mathbb{C}^N), \quad \psi(k) := \sum_{x \in V(\hat{G}) \setminus T} \sum_{j=0}^{N-1} \psi_j(x; k) |x\rangle \langle 0, j| \in \text{Hom}(\mathbb{C}^N, \mathbb{C}^M), \quad (\text{A6})$$

and the matrix consisting of $A \in \text{End}(\mathbb{C}^N)$, $D \in \text{End}(\mathbb{C}^M)$, and $B \in \text{Hom}(\mathbb{C}^N, \mathbb{C}^M)$ is the adjacency matrix $\mathcal{A}(\hat{G})$: $A = A^\dagger$ and $D = D^\dagger$ are the adjacency matrices of the N terminal vertices and the M internal vertices, respectively, and B is the adjacency matrix between the terminal and the internal vertices. Solving (A5), one straightforwardly finds

$$S(k) = -e^{2ik} Q^{-1}(k) Q(-k), \quad Q(k) := \left[1 - e^{ik} \left(A + B^\dagger \frac{1}{2 \cos k - D} B \right) \right]. \quad (\text{A7})$$

For $k \in \mathbb{R}$, the S matrix satisfies

$$S(k)^\dagger S(k) = S(-k) S(k) = 1 \quad (k \in \mathbb{R}), \quad (\text{A8})$$

which can be easily seen by noting that A and D are Hermitian, $Q(k)^\dagger = Q(-k)$, and $[Q(k), Q(-k)] = 0$.

Finally, let us show that the single-particle S matrix of the blue walker ($c = 1$) [denote it by $\tilde{S}(k)$] is given by $\tilde{S}(k) = S(k)^\text{T}$ for $k \in \mathbb{R}$, which is the transpose of the S matrix of the red walker. By the property (2.13), $\tilde{S}(k)$ can be obtained by simply replacing $\mathcal{A}(\hat{G})$ with $\mathcal{A}(\hat{G})^*$. More explicitly, it is given by replacing $\{A, B, D\}$ with $\{A^*, B^*, D^*\}$ in (A7). This replacement changes $S(k)$ to $S(-k)^*$ ($k \in \mathbb{R}$). Using $S(k)^\dagger = S(-k)$ ($k \in \mathbb{R}$) derived from (A8), we arrive at

$$\tilde{S}(k) = S(-k)^* = [S(k)^\dagger]^* = S(k)^\text{T}. \quad (\text{A9})$$

2. Two-particle scattering on an infinite path

Next we consider the two-particle scattering on an infinite path: The walker (wave packet) with a momentum close to a specific value of $k_0 \in (-\pi, 0)$ moves right (down) toward the walker which moves left (up) with a momentum close to $k_1 \in (0, \pi)$. Since, in our architecture, we are concerned with the scattering of red walkers, here we only consider the spatial part of the states as in the single-particle scattering. The two-particle scattering process can be characterized by the scattering state $|\psi(k_0, k_1)\rangle$ with definite values of (k_0, k_1) . More explicitly,

$$|\psi(k_0, k_1)\rangle = \sum_{x_0, x_1 \in \mathbb{Z}} \psi(x_0, x_1; k_0, k_1) |x_0, x_1\rangle, \quad (\text{A10})$$

where $x_0, x_1 \in \mathbb{Z}$ are vertices on an infinite path and the wave function $\psi(x_0, x_1; k_0, k_1)$ is written as

$$\begin{aligned} \psi(x_0, x_1; k_0, k_1) &= \begin{cases} e^{ik_0 x_0 + ik_1 x_1} \pm S_{01}(k_0, k_1) e^{ik_1 x_0 + ik_0 x_1} & (x_0 < x_1) \\ S_{01}(k_0, k_1) e^{ik_0 x_0 + ik_1 x_1} \pm e^{ik_1 x_0 + ik_0 x_1} & (x_0 > x_1). \end{cases} \end{aligned} \quad (\text{A11})$$

Here $S_{01} \in \mathbb{C}$ is the scattering amplitude and the $+$ and $-$ signs correspond to bosons and fermions, respectively. For the bosonic case, $\psi(x, x)$ is given by setting formally $x_0 = x_1 = x$ in Eq. (A11).

The form of the wave function (A11) is followed by the following facts.

(i) The individual momenta k_0 and k_1 are conserved after the scattering, due to the conservation law of the total energy $2(\cos k_0 + \cos k_1)$ and momentum $k_0 + k_1$. The two walkers only acquire a phase factor $S_{01}(k_0, k_1)$ after the scattering.

(ii) The wave function is symmetric (antisymmetric) under particle exchange, reflecting the Bose (Fermi) statistics.

(iii) Interactions are limited to on-site or nearest-neighbor pairs.

Indeed, for $x_0 \neq x_1$ ($x_0 \neq x_1 + 1$) in the bosonic (fermionic) case, one can easily check that the wave function (A11) satisfies the Schrödinger equation

$$\langle x_0, x_1 | \mathcal{H}_G | \psi(k_0, k_1) \rangle = 2(\cos k_0 + \cos k_1) \psi(x_0, x_1; k_0, k_1), \quad (\text{A12})$$

where \mathcal{H}_G [Eq. (2.10)] with the interaction term (2.15) is defined on an infinite path, i.e., $\theta_{jk} = 0$. Below, solving (A12) at $x_0 = x_1$ ($x_0 = x_1 - 1$) for the bosonic (fermionic) case, we determine the scattering amplitude $S_{01}(k_0, k_1)$.

a. Bosonic walkers

We adopt the on-site (Bose-Hubbard) interaction (2.15) for the bosonic quantum walkers. The left-hand side of the Schrödinger equation (A12) at $x_0 = x_1 =: x$ gives

$$\begin{aligned} & \psi(x, x+1; k_0, k_1) + \psi(x-1, x; k_0, k_1) \\ & + \psi(x, x-1; k_0, k_1) + \psi(x+1, x; k_0, k_1) \\ & + u\psi(x, x; k_0, k_1) \\ & = [2(e^{ik_1} + e^{-ik_0}) + u + S_{01}(k_0, k_1)\{2(e^{ik_0} + e^{-ik_1}) + u\}] \\ & \times e^{i(k_0+k_1)x}. \end{aligned} \quad (\text{A13})$$

Because the right-hand side of (A12) is given by

$$2(\cos k_0 + \cos k_1)[1 + S_{01}(k_0, k_1)]e^{i(k_0+k_1)x}, \quad (\text{A14})$$

we arrive at

$$S_{01}(k_0, k_1) = \frac{2(\sin k_0 - \sin k_1) + iu}{2(\sin k_0 - \sin k_1) - iu}. \quad (\text{A15})$$

b. Fermionic walkers

For the fermionic quantum walkers, we employ the nearest-neighbor interaction (2.15). The left-hand side of the Schrödinger equation (A12) at $x_0 = x_1 - 1 =: x$ gives

$$\begin{aligned} & \psi(x-1, x+1; k_0, k_1) + \psi(x, x+2; k_0, k_1) \\ & + u\psi(x, x+1; k_0, k_1) \\ & = \{(e^{ik_1} + e^{-ik_0} + u)e^{ik_1} - S_{01}(k_0, k_1) \\ & \times [(e^{ik_0} + e^{-ik_1} + u)e^{ik_0}]\} e^{i(k_0+k_1)x}. \end{aligned} \quad (\text{A16})$$

Also, we find the right-hand side of (A12) is given by

$$2(\cos k_0 + \cos k_1)[e^{ik_1} - S_{01}(k_0, k_1)e^{ik_0}]e^{i(k_0+k_1)x}, \quad (\text{A17})$$

and therefore

$$S_{01}(k_0, k_1) = \frac{1 + e^{i(k_0+k_1)} - e^{ik_1}u}{1 + e^{i(k_0+k_1)} - e^{ik_0}u}. \quad (\text{A18})$$

-
- [1] N. Konno, Quantum random walks in one dimension, *Quantum Inf. Process.* **1**, 345 (2002).
- [2] J. Kempe, Quantum random walks: An introductory overview, *Contemp. Phys.* **44**, 307 (2003).
- [3] A. Ambainis, Quantum walks and their algorithmic applications, *Int. J. Quantum Inf.* **01**, 507 (2003).
- [4] V. Kendon, Decoherence in quantum walks—A review, *Math. Struct. Comput. Sci.* **17**, 1169 (2007).
- [5] N. Konno, in *Quantum Potential Theory*, edited by U. Franz and M. Schürmann, Lecture Notes in Mathematics Vol. 1954 (Springer, Berlin, 2008), pp. 309–452.
- [6] S. E. Venegas-Andraca, in *Quantum Walks for Computer Scientists*, edited by M. Lanzagorta and J. Uhlmann, Synthesis Lectures on Quantum Computing (Springer, Berlin, 2008), Vol. 1.
- [7] S. E. Venegas-Andraca, Quantum walks: A comprehensive review, *Quantum Inf. Process.* **11**, 1015 (2012).
- [8] J. Wang and K. Manouchehri, *Physical Implementation of Quantum Walks* (Springer, Berlin, 2013).
- [9] R. Portugal, *Quantum Walks and Search Algorithms* (Springer, Berlin, 2013).
- [10] C. Moore and A. Russell, in *Proceedings of the Sixth International Workshop on Randomization and Approximation Techniques in Computer Science, Cambridge*, edited by J. D. P. Rolim and S. Vadhan (Springer, Berlin, 2002), pp. 164–178.
- [11] N. Shenvi, J. Kempe, and K. Birgitta Whaley, Quantum random-walk search algorithm, *Phys. Rev. A* **67**, 052307 (2003).
- [12] I. Carneiro, M. Loo, X. Xu, M. Girerd, V. Kendon, and P. L. Knight, Entanglement in coined quantum walks on regular graphs, *New J. Phys.* **7**, 156 (2005).
- [13] A. M. Childs, R. Cleve, E. Deotto, E. Farhi, S. Gutmann, and D. A. Spielman, in *Proceedings of the 35th Annual ACM Symposium on Theory of Computing* (ACM Press, New York, 2003), pp. 59–68.
- [14] B. Tregenna, W. Flanagan, R. Maile, and V. Kendon, Controlling discrete quantum walks: Coins and initial states, *New J. Phys.* **5**, 83 (2003).
- [15] A. Ambainis, Quantum walk algorithm for element distinctness, *SIAM J. Comput.* **37**, 210 (2007).
- [16] P. C. Richter, Almost uniform sampling via quantum walks, *New J. Phys.* **9**, 72 (2007).
- [17] H. Gerhardt and J. Watrous, in *Random'03: Proceedings of the 7th International Workshop on Randomization and Approximation Techniques in Computer Science, Princeton*, Lecture Notes in Computer Science Vol. 2764 (Springer, New York, 2003), pp. 290–301.
- [18] S.-y. Shiao, R. Joynt, and S. N. Coppersmith, Physically-motivated dynamical algorithms for the graph isomorphism problem, *Quantum Inf. Comput.* **5**, 492 (2005).
- [19] B. L. Douglas and J. B. Wang, A classical approach to the graph isomorphism problem using quantum walks, *J. Phys. A: Math. Theor.* **41**, 075303 (2008).
- [20] J. K. Gamble, M. Friesen, D. Zhou, R. Joynt, and S. N. Coppersmith, Two-particle quantum walks applied to the graph isomorphism problem, *Phys. Rev. A* **81**, 052313 (2010).
- [21] S. D. Berry and J. B. Wang, Two-particle quantum walks: Entanglement and graph isomorphism testing, *Phys. Rev. A* **83**, 042317 (2011).
- [22] A. M. Childs, Universal Computation by Quantum Walk, *Phys. Rev. Lett.* **102**, 180501 (2009).

- [23] A. M. Childs, D. Gosset, and Z. Webb, Universal computation by multiparticle quantum walk, *Science* **339**, 791 (2013).
- [24] N. B. Lovett, S. Cooper, M. Everitt, M. Trevers, and V. Kendon, Universal quantum computation using the discrete-time quantum walk, *Phys. Rev. A* **81**, 042330 (2010).
- [25] M. S. Underwood and D. L. Feder, Universal quantum computation by discontinuous quantum walk, *Phys. Rev. A* **82**, 042304 (2010).
- [26] D. Reitzner, D. Nagaj, and V. Buzek, Quantum walks, *Acta Phys. Slovaca* **61**, 603 (2011).
- [27] N. Bao, P. Hayden, G. Salton, and N. Thomas, Universal quantum computation by scattering in the Fermi-Hubbard model, *New J. Phys.* **17**, 093028 (2015).
- [28] K. F. Thompson, C. Gokler, S. Lloyd, and P. W. Shor, Time independent universal computing with spin chains: Quantum Plinko machine, *New J. Phys.* **18**, 073044 (2016).
- [29] E. Piccinini, C. Benedetti, I. Siloi, M. G. A. Paris, and P. Bordone, GPU-accelerated algorithms for many-particle continuous-time quantum walks, *Comput. Phys. Commun.* **215**, 235 (2017).
- [30] M. Ezawa, Electric-circuit simulation of the Schrödinger equation and non-Hermitian quantum walks, *Phys. Rev. B* **100**, 165419 (2019).
- [31] M. Tamura, T. Mukaiyama, and K. Toyoda, Quantum Walks of a Phonon in Trapped Ions, *Phys. Rev. Lett.* **124**, 200501 (2020).
- [32] M. Ezawa, Electric circuits for universal quantum gates and quantum Fourier transformation, *Phys. Rev. Res.* **2**, 023278 (2020).
- [33] S. Singh, P. Chawla, A. Sarkar, and C. M. Chandrashekar, Universal quantum computing using single-particle discrete-time quantum walk, *Sci. Rep.* **11**, 11551 (2021).
- [34] R. Asaka, K. Sakai, and R. Yahagi, Quantum random access memory via quantum walk, *Quantum Sci. Technol.* **6**, 035004 (2021).
- [35] R. Asaka, K. Sakai, and R. Yahagi, Two-level quantum walkers on directed graphs. II. Application to quantum random access memory, following paper, *Phys. Rev. A* **107**, 022416 (2023).
- [36] A. M. Childs and D. Gosset, Levinson's theorem for graphs II, *J. Math. Phys.* **53**, 102207 (2012).
- [37] Y. Aharonov and A. Casher, Topological Quantum Effects for Neutral Particles, *Phys. Rev. Lett.* **53**, 319 (1984).
- [38] A. A. Zvyagin and I. V. Krive, Aharonov-Casher effect in the Hubbard model with repulsion, *Zh. Eksp. Teor. Fiz.* **102**, 1376 (1992) [*Sov. Phys. JETP* **75**, 745 (1992)].
- [39] M. A. Nielsen and I. L. Chuang, *Quantum Computation and Quantum Information: 10th Anniversary Edition*, 10th ed. (Cambridge University Press, New York, 2011).
- [40] C. P. Williams, *Explorations in Quantum Computing* (Springer, Berlin, 2011), pp. 51–122.
- [41] E. Farhi, J. Goldstone, and S. Gutmann, A quantum algorithm for the Hamiltonian NAND tree, *Theory Comput.* **4**, 169 (2008).
- [42] L. K. Grover, in *Proceedings of the 28th Annual ACM Symposium on Theory of Computing, Philadelphia* (ACM Press, New York, 1996), pp. 212–219.
- [43] P. W. Shor, in *Proceedings of the 35th Annual Symposium on Foundations of Computer Science, Santa Fe* (IEEE, Piscataway, 1994), pp. 124–134.
- [44] R. Asaka, K. Sakai, and R. Yahagi, Quantum circuit for the fast Fourier transform, *Quantum Inf. Process.* **19**, 277 (2020).